Autophagy inhibition-mediated epithelial-mesenchymal transition augments local myofibroblast differentiation in pulmonary fibrosis

Charlotte Hill[1,11], Juanjuan Li[1,11], Dian Liu[2], Franco Conforti[3,4], Christopher J. Brereton[3,4], Liudi Yao[1], Yilu Zhou[1], Aiman Alzetani[4,5], Serena J. Chee[5,6], Ben G. Marshall[4,5], Sophie V. Fletcher[4,5], David Hancock[7], Christian H. Ottensmeier[6], Andrew J. Steele[6], Julian Downward[7], Luca Richeldi[3,4,8], Xin Lu[9], Donna E. Davies[3,4,10], Mark G. Jones[3,4], and Yihua Wang[1,2,10]

[1]Biological Sciences, Faculty of Environmental and Life Sciences, University of Southampton, Southampton SO17 1BJ, UK. [2]Department of Oncology, Tongji Hospital, Tongji Medical College, Huazhong University of Science and Technology, Wuhan, China. [3]Clinical and Experimental Sciences, Faculty of Medicine, University of Southampton, Southampton SO16 6YD, UK. [4]NIHR Southampton Biomedical Research Centre, University Hospital Southampton, Southampton SO16 6YD, UK. [5]University Hospital Southampton, Southampton SO16 6YD, UK. [6]Cancer Sciences & NIHR and CRUK Experimental Cancer Sciences Unit, University of Southampton, Southampton SO16 6YD, UK. [7]Oncogene Biology, The Francis Crick Institute, London NW1 1AT, UK. [8]Unità Operativa Complessa di Pneumologia, Università Cattolica del Sacro Cuore, Fondazione Policlinico A. Gemelli, Rome, Italy. [9]Ludwig Institute for Cancer Research, Nuffield Department of Clinical Medicine, University of Oxford, Oxford OX3 7DQ, UK. [10]Institute for Life Sciences, University of Southampton, Southampton SO17 1BJ, UK. [11]These authors contributed equally to this work.

Correspondence should be addressed to Y.W. (e-mail: yihua.wang@soton.ac.uk).

Running title: Autophagy inhibition in IPF

Abstract

Idiopathic pulmonary fibrosis (IPF), the prototypic progressive fibrotic interstitial lung disease, is thought to be a consequence of repetitive micro-injuries to an ageing, susceptible alveolar epithelium. Ageing is a risk factor for IPF and incidence has been demonstrated to increase with age. Decreased (macro)autophagy with age has been reported extensively in a variety of systems and diseases, including IPF. However, it is undetermined whether the role of faulty autophagy is causal or coincidental in the context of IPF. Here we report that in alveolar epithelial cells inhibition of autophagy promotes epithelial-mesenchymal transition (EMT), a process implicated in embryonic development, wound healing, cancer metastasis and fibrosis. We further demonstrate that this is attained, at least in part, by increased p62/SQSTM1 expression that promotes p65/RELA mediated-transactivation of an EMT transcription factor, Snail2 (*SNAI2*), which not only controls EMT but also regulates the production of locally acting profibrogenic mediators. Our data suggest that reduced autophagy induces EMT of alveolar epithelial cells and can contribute to fibrosis via aberrant epithelial–fibroblast crosstalk.

Introduction

Idiopathic pulmonary fibrosis (IPF) is the most common type of chronic, progressive fibrotic interstitial lung disease. It occurs with comparable incidence to that of stomach, brain, and testicular cancer[1], and the median survival of patients with IPF is only 3 years[2,3]. IPF is characterised by aberrant extracellular matrix (ECM) deposition, which leads to decreased lung compliance, disrupted gas-exchange, and ultimately respiratory failure and death. As approved therapies only slow disease progression there is significant unmet medical need.

Evidence suggests that interacting genetic and environmental factors are crucial for the development of IPF, with repetitive injuries to aged alveolar epithelium thought to play an important role[2]. Ageing is a risk factor for IPF, with disease incidence increasing with age[3]. Decreased (macro)autophagy with age has been reported extensively in a variety of systems and diseases[4], including IPF[5–9]. Autophagy is a tightly controlled, evolutionarily conserved process for the lysosomal degradation of cytoplasmic cargo, long-lived proteins and organelles. Growing evidence suggests that autophagy acts as an adaptive response to facilitate cell survival and limit cell death following exposure to stressful stimuli[10].

Tissues from IPF patients are characterised by defective autophagy responses[5–8], although it is unclear whether faulty autophagy exerts an effect directly, or if this change is merely coincident with IPF. Loss of *autophagy-related protein 7 (ATG7)*, a ubiquitin-activating enzyme that is essential for autophagy, has been demonstrated both *in vivo* and *in vitro* to induce endothelial-to-mesenchymal transition (EndMT). Autophagy inhibition, by loss of *ATG7*, has been associated with changes in endothelial cell (EC) architecture, reduced endothelial markers and increased mesenchymal markers, whilst EC-specific *Atg7* knock-out mice had increased susceptibility to bleomycin induced-fibrosis[11]. Furthermore, inhibition of autophagy is sufficient to induce acceleration of both bronchial epithelial cell senescence and differentiation of lung fibroblasts into myofibroblasts[8]. Here we report that autophagy

inhibition promotes epithelial-mesenchymal transition (EMT) in alveolar epithelial cells. EMT is a reversible biological process where epithelial cells gain migratory and invasive abilities through loss of cell polarity and cadherin-mediated cell-cell adhesion; this process has been implicated in embryonic development, wound healing, cancer metastasis and organ fibrosis[12]. Specific transcription factors, EMT transcription factors (EMT-TFs) including Snail, ZEB and TWIST are able to promote the repression of epithelial features and induction of mesenchymal features[13,14]. We show that promotion of EMT by autophagy inhibition in alveolar epithelial cells is attained, at least in part, by increased p62/SQSTM1 expression that induces p65/RELA mediated-transactivation of Snail2 (*SNAI2*), which not only controls EMT but also regulates the production of locally acting profibrogenic mediators. This suggests that autophagy inhibition-induced EMT of alveolar epithelial cells contributes to fibrosis not only by affecting the epithelial phenotype but also via aberrant epithelial–fibroblast crosstalk.

Results

Autophagic activity is down regulated in IPF lungs.

Defective autophagy responses in tissues from IPF patients have been reported previously[6,8]. Similarly, we observed evidence of autophagy inhibition as determined by p62/SQSTM1 accumulation in lung epithelial cells in IPF samples (Fig. 1; Supplementary Fig. S1a). p62/SQSTM1 is a key protein involved in autophagy that recognises cellular waste which is then sequestered and degraded by autophagy[15]. A strong staining for p62/SQSTM1 was detected in IPF tissue within epithelial cells of thickened alveoli septae where collagen deposition in the interstitium was demonstrated (Fig. 1b; Supplementary Fig. S1a), as well as within fibroblastic foci (Fig. 1a). In contrast, there was weak p62/SQSTM1 expression and little collagen deposition detected in alveoli of control lung tissue (Fig. 1c). Using a publicly available dataset[16], the mRNA level of *SQSTM1* (p62) in IPF epithelial cells was evaluated. It was found that *SQSTM1* (p62) mRNA expression level was reduced in IPF lungs (Supplementary Fig. S1b) whilst its protein level as assessed by immunohistochemistry was increased in IPF (Fig. 1b; Supplementary Fig. S1a). Given that p62/SQSTM1 protein levels are predominantly regulated by autophagic activity[17], these results suggest that autophagic activity is down regulated in IPF epithelial cells.

Alteration of autophagic activity affects cellular plasticity of alveolar epithelial cells.

To investigate its role in alveolar epithelial cells, autophagic activity was first modified using chemical inhibitors. We treated human alveolar epithelial type II (ATII) cells[18–20] with an autophagy inhibitor, hydroxychloroquine (HCQ), which is a lysosomotropic autophagy inhibitor. HCQ treatment of ATII cells inhibited autophagic activity, demonstrated by the accumulation of p62/SQSTM1 (Fig. 2a), inhibition of lysosomal degradation by HCQ also caused accumulation of LC3-II (Fig. 2a). Autophagy inhibition with HCQ resulted in a down-

regulation of E-cadherin in a time-dependent manner (Fig. 2a). Morphology changes were also observed following HCQ treatment with ATII cells developing an elongated mesenchymal cell phenotype; this was accompanied by actin cytoskeleton reorganisation demonstrated using filamentous actin (F-actin) staining with Phalloidin (Fig. 2c), suggesting induction of a cellular reprogramming process, EMT. A group of transcription factors, termed EMT-TFs, are capable of inducing EMT, these include Snail1 (*SNAI1*), Snail2 (*SNAI2*), TWIST1, ZEB1 and ZEB2[13], which act by binding E-boxes in the proximal promoter of the *CDH1* (E-cadherin) gene to repress its expression. We thus investigated the impact of HCQ treatment on the mRNA expression levels of E-cadherin (*CDH1*) and EMT-TFs in ATII cells. Following HCQ treatment of ATII cells, we observed a down-regulation of E-cadherin (*CDH1*), increased levels of a mesenchymal marker Vimentin (*VIM*) and an EMT-TF Snail2 (*SNAI2*), but not others (Fig. 2b).

To confirm our observations with HCQ, we treated ATII cells with another autophagy inhibitor, Bafilomycin-A1 (Baf-A1), which inhibits autophagy by disrupting vesicular acidification leading to an accumulation of mature, undigested autophagosomes[21]. Autophagy inhibition by Baf-A1 treatment of ATII cells resulted in a similar induction of EMT, evidenced by a reduction in E-cadherin (Supplementary Fig. S2a), an increase of Vimentin (*VIM*) (Supplementary Fig. S2b), and an up-regulation of EMT-TF Snail2 (*SNAI2*) (Supplementary Fig. S2a and b). Morphology changes were observed following Baf-A1 treatment of ATII cells, with cells developing invasive phenotype when cultured in Matrigel (Supplementary Fig. S2c).

We further used small interfering RNAs (siRNAs) against *autophagy-related protein 5* (*ATG5*) to study the effects of inhibition of autophagic activity in ATII cells. ATG5, a ubiquitin-protein ligase (E3)-like enzyme, is essential for autophagy due to its role in autophagosome elongation. *ATG5* siRNA-transfection of ATII cells inhibited autophagic

activity, evidenced by the accumulation of p62/SQSTM1 (Fig. 3a and c). As a result, *ATG5* depletion led to a down-regulation of E-cadherin at both the mRNA and protein levels (Fig. 3a and b), an increase in *VIM* (Vimentin) at mRNA levels (Fig. 3b), and a rearrangement of the F-actin cytoskeleton (Fig. 3c). Similar results were observed in A549 alveolar epithelial cells where autophagy inhibition by *ATG5* depletion down regulated E-cadherin levels and increased Snail2 (*SNAI2*) expression (Supplementary Fig. S3a-c).

In a wound healing context, the EMT process allows epithelial cells to adopt a more migratory mesenchymal phenotype in order to spread rapidly and cover the wounded area[22]. Therefore, a wound scratch assay was utilised to test whether *ATG5* depletion using *ATG5* siRNA was sufficient to augment cell mobility. This showed that 20 h after creating the scratch wound, *ATG5* siRNA-transfected ATII cells had more completely repaired the wound compared to control siRNA transfected cells (Fig. 3d; $P < 0.001$). In addition, we found in both the Transwell migration (Fig. 3e) and Matrigel invasion assays (Supplementary Fig. S3d), knockdown of *ATG5* promoted cell migration and invasion, respectively.

Having examined the effects of autophagy inhibition in ATII cells, we next evaluated the effect of autophagy induction using Rapamycin, which inhibits mammalian Target Of Rapamycin (mTOR)[23]. As predicted, following Rapamycin treatment of ATII cells, phosphorylation levels of mTOR were reduced (Supplementary Fig. S4a), and autophagy activity was induced, indicated by a down-regulation of p62/SQSTM1 and an increase in LC3-II (Supplementary Fig. S4a). We also found an increase in *CDH1* (E-cadherin), and reductions in *VIM* (Vimentin) and *SNAI2* (Snail2) mRNA levels in ATII cells treated with Rapamycin (Supplementary Fig. S4b), and these effects were mainly via the induction of autophagy, since knockdown of *ATG5* completely abolished the changes (Supplementary Fig. S4b).

Together, our results demonstrate that autophagic activity is an important regulator of cellular plasticity in alveolar epithelial cells.

Autophagy inhibition induces EMT via p62/SQSMT1-NFκB-Snail2 pathway in alveolar epithelial cells.

We recently reported that in colorectal and pancreatic cancer cells, inhibition of autophagy induces EMT via p62/SQSMT1-NFκB pathway[24]. Therefore, we investigated if this pathway is involved in initiating autophagy inhibition-induced EMT in ATII cells. Comparison of control and HCQ-treated cells revealed that p65/RELA accumulated in the nuclei of treated cells (Fig. 4a), indicating that the NF-κB pathway is activated in ATII cells when autophagy is inhibited. Functionally, p62/*SQSTM1* or p65/*RELA* knockdown abolished the increase in Snail2 following autophagy inhibition by HCQ treatment in ATII cells (Fig. 4b). Similar results were observed in A549 cells (Supplementary Fig. S5). While knockdown of *ATG5* induced EMT, as evidenced by a reduction in *CDH1* (E-cadherin) mRNA levels and increased *SNAI2* (Snail2) mRNA levels, subsequent depletion of *RELA* (p65) or *SQSTM1* (p62) (Supplementary Fig. S5a) partially or completely abolished the increase in *SNAI2* (Snail2), and restored *CDH1* (E-cadherin) expression (Supplementary Fig. S5b). These data suggest that autophagy inhibition in alveolar epithelial cells promotes EMT via the p62/SQSMT1-NFκB-Snail2 pathway.

ATII cells undergoing autophagy inhibition-induced EMT induce fibroblast activation via Snail2-regulated paracrine signalling.

Given that autophagy inhibition is able to induce EMT in ATII cells, we wanted to determine the role of these cells in the context of fibrosis, and whether they were contributing to the fibroblast population directly. Comparison of ECM components in control or *ATG5* siRNA

ATII cells demonstrated that ATII cells after autophagy inhibition-induced EMT did not express significantly more ECM genes (Supplementary Fig. S6). This suggested ECM production in IPF lung tissue (Fig. 1) was unlikely due directly to EMT but rather epithelial cells exhibiting an indirect effect on fibrogenesis. Therefore we investigated whether *ATG5*-depleted ATII cells could produce secreted factors that activate fibroblasts. We treated primary human lung fibroblasts from IPF patients (IPF fibroblasts, IPFFs) with conditioned media (CM) from ATII cells transfected with control or *ATG5* siRNA (Fig. 5a) without or with addition of transforming growth factor-β (TGF-β), and assessed levels of α-smooth muscle actin (α-SMA), a marker of myofibroblast differentiation. CM from ATII cells transfected with *ATG5* siRNA without TGF-β had minimal effect on the activation of fibroblasts (Fig. 5b). However in IPFFs, CM from *ATG5*-depleted ATII cells together with TGF-β achieved a synergistic effect in activating fibroblasts as assessed by α-SMA protein levels (Fig. 5b). Notably, levels of phospho-Smad2 (p-Smad2) did not significantly change between different CM with TGF-β treatment, suggesting α-SMA increase may be Smad2-independent (Fig. 5b). Given the importance of Snail2 (*SNAI2*) in mediating EMT by autophagy inhibition (Fig. 5a), we hypothesised that Snail2 (*SNAI2*) may facilitate crosstalk by mediating paracrine signalling from ATII cells undergoing autophagy inhibition-induced EMT. Snail2 (*SNAI2*) depletion (Fig. 5a) in ATII cells eliminated the effects of CM from *ATG5*-depleted ATII cells on activation of fibroblasts in the presence of TGF-β (Fig. 5c), highlighting the importance of Snail2 (*SNAI2*) as a key regulator of paracrine signalling between alveolar cells and fibroblasts in IPF under conditions where autophagy is defective.

Discussion

Fibrotic diseases are poorly characterised and lack effective treatment[25], with fibrosis presenting as a pathological feature in a range of disease affecting many organs[25,26]. A rise in the incidence of some fibrotic diseases[1,3] and with fibrogenesis being accepted as a major cause of death[27]; it is evident that they are becoming an increasing health-care burden, requiring further research to elucidate underlying mechanisms which drive fibrogenesis. IPF is an aging-associated chronic, interstitial lung disease[2,28–34]. Treatment options for patients are limited[35] and the underlying mechanisms for fibrosis are still debated[36]. EMT has been suggested to have a direct role in fibrosis human IPF, with studies showing co-localisation of epithelial and mesenchymal markers[37–41], and laser capture micro-dissection isolated RNA from epithelial cells in IPF lungs and confirmed expression of mesenchymal markers[42]. However, lineage tracing studies found the number of fibroblasts derived from epithelial cells to be small[43,44] and these cells were not found to co-localise with α-SMA suggesting they did not transition to myofibroblasts[45,46]. It also been proposed in a number of systems that epithelial cells that have undergone EMT may secrete a range of fibrogenic growth factors and cytokines, with impaired epithelial repair leading to aberrant epithelial mesenchymal communication contributing to the recruitment and activation of myofibroblasts[18,47,48]. Here we show that autophagy inhibition in ATII cells can induce EMT, and this contributes to fibrosis via aberrant epithelial-fibroblast crosstalk, rather than as a direct contribution to the fibroblast population.

Autophagy is a tightly controlled, evolutionarily conserved biological process where long-lived proteins and damaged organelles are degraded. Manipulation of autophagy is now being utilised as a therapeutic approach in a number of fields, such as, neurodegenerative diseases and cancer[49,50]. On the other hand, decreased autophagic activity has been reported in many human diseases[51], including IPF[5–8]. In IPF, ageing is a main risk factor in its development

with patients under the age of 50 being rare[29]. Ageing has been linked to reduced autophagy in many contexts including IPF[5,52]. Consistent with these findings[6,8] we demonstrated strong immunostaining for p62/SQSTM1 in IPF epithelial cells of thickened alveolar septae whilst identifying only very weak signals in the control lung. We found significantly lower levels of *SQSTM1* (p62) mRNA in IPF epithelial cells compared to control epithelial cells, which indicated that the increase in p62/SQSTM1 protein levels was due to reduced autophagic activity. Taken with previous findings[6,8], these results indicate that autophagic activity is down regulated in IPF epithelial cells.

Whilst the concept of EMT is well established in the context of embryonic development, it also plays a role in in wound healing, cancer metastasis and fibrosis[12]. EMT requires a complex orchestration of multiple signalling pathways, including TGF-β, fibroblast growth factor (FGF), Wnt/β-catenin, epidermal growth factor (EGF) and others. Loss of E-cadherin is considered to be a fundamental event in EMT. Snail1/2, ZEB1/2 and some basic helix-loop-helix (bHLH) factors are potent repressors of E-cadherin expression[53,54]. The role of EMT in cancer is detrimental whereas in wound healing, EMT as a response to injury can be beneficial, however if the wound healing process is exaggerated it may lead to fibrosis. The interplay between autophagy and EMT have been reported in other disease contexts[55–57], with a recent study demonstrating inhibition of autophagy induces EMT via p62/SQSMT1-NFκB/RELA pathway in *RAS*-mutated cancer cells[24]. This is mainly via up-regulation of ZEB1 and to a lesser extent via Snail2[24]. In contrast, in lung alveolar epithelial cells, autophagy inhibition induces EMT in the absence of RAS activation and is exclusively via up-regulation of Snail2 (Fig. 6a), indicating this effect is likely dependent on the cellular context. The importance of Snail2 in IPF has been demonstrated with Snail2 being up-regulated in IPF lung epithelial cells, but not Snail1 or TWIST1, compared to control epithelial cells[16,18]. Jayachandran *et al.* reported that Snail2-mediated EMT may contribute to

the fibroblast pool[54]. However, in this study, we found ATII cells undergoing autophagy inhibition-induced EMT induce fibroblast activation via Snail2-regulated paracrine signalling.

In IPF it was recently reported that micro-injuries could lead to the activation of the EGFR-RAS-ERK pathway, and ZEB1 was demonstrated to mediate paracrine signalling[18]. Similarly in renal fibrosis, tubular epithelial cells are able to promote myofibroblast differentiation and fibrogenesis without directly contributing to the fibroblast population by relaying signals to the interstitium. For example, in a murine model, damage-mediated Snail1 reactivation induced partial EMT and resulted in renal fibrosis, but these cells did not contribute to myofibroblast or interstitial cell population[47]. Conversely, EMT was inhibited and interstitial fibrosis attenuated upon conditional deletion of *Snail1* or *Twist1*[48].

Taken together, we believe that repetitive local micro-injuries to ageing alveolar epithelium cause persistent activation of alveolar epithelial cells, which secrete numerous profibrogenic factors, driving local myofibroblast differentiation (Fig. 6b). Thus, targeting of EMT inducers might have therapeutic potential in fibrotic conditions, with such therapies currently undergoing development in the context of malignancy[58,59].

Methods

Lung tissue sampling. All human lung experiments were approved by the Southampton and South West Hampshire and the Mid and South Buckinghamshire Local Research Ethics Committees, and all subjects gave written informed consent. Clinically indicated IPF lung biopsy tissue samples and non-fibrotic control tissue samples (macroscopically normal lung sampled remote from a cancer site) were assessed as surplus to clinical diagnostic requirements. All IPF samples were from patients subsequently receiving a multidisciplinary diagnosis of IPF according to international consensus guidelines[29].

Cell culture, reagents and transfections. Primary parenchymal lung fibroblast cultures were established from IPF tissues as described previously[60,61]. Fibroblasts were cultured in Dulbecco's Modified Eagle's Medium (DMEM) supplemented with 10% foetal bovine serum (FBS), 50 units/ml penicillin, 50μg/ml streptomycin, 2mM L-glutamine, 1mM sodium pyruvate and 1x non-essential amino acids (DMEM/FBS) (all from Life Technologies. ATII cells[18–20] were cultured in DCCM-1 (Biological Industries Ltd) supplemented with 10% NBCS (Life Technologies), 1% penicillin, 1% streptomycin and 1% L-glutamine (all from Sigma Aldrich). A549 cells were cultured in DMEM (Fisher Scientific UK, 11594446) supplemented with 10% FBS (Invitrogen) and antibiotics. All cells were kept at 37 °C and 5% CO_2. For 3D culture, ATII cells were cultured as previously described[62] in Matrigel (BD Biosciences). Bafilomycin-A1 (Baf-A1) was from Enzo Life Sciences. Hydroxychloroquine (HCQ) and Rapamycin were from Sigma Aldrich. No mycoplasma contamination was detected in the cell lines used.

Short interfering RNA (siRNA) oligos against *ATG5* (MU-004374-04-0002), *SQSTM1* (p62) (MU-010230-00-0002), *SNAI2* (Snail2) (MU-017386-00-0002) and *RELA* (p65) (MU-

003533-02-0002) were purchased from Dharmacon. Sequences are available from Dharmacon, or on request. As a negative control we used siGENOME RISC-Free siRNA (Dharmacon, D-001220–01). ATII and A549 cells were transfected with the indicated siRNA oligos at a final concentration of 35 nM using DharmaFECT 2 reagent (Dharmacon).

Western blot analysis. Western blot analysis was performed with lysates from cells with urea buffer (8 M Urea, 1 M Thiourea, 0.5% CHAPS, 50 mM DTT, and 24 mM Spermine). Primary antibodies were from: Santa Cruz (β-actin, sc-47778; E-cadherin, sc-21791; Snail2, sc-10436), Abcam (β-tubulin, ab6046), Cell Signalling Technology (α-SMA, 14968; Snail2, 9585; Smad2, 5339; Phospho-Smad2, 3104; β-tubulin, 86298; LC3, 2775; p62/SQSTM1, 5114; p65/RELA, 8242; ATG5, 2630; mTOR, 2972; Phospho-mTOR Ser2448, 5536), and BD Transduction Laboratories (E-cadherin, 610405). Signals were detected using an ECL detection system (GE Healthcare) or Odyssey imaging system (LI-COR), and evaluated by ImageJ 1.42q software (National Institutes of Health).

qRT-PCR. Total RNA was isolated using RNeasy mini kit (Qiagen) according to manufacturer's instructions and quantified using a Nanodrop Spectophotometer 2000c (Thermo Fisher Scientific). Real-time quantitative RT-PCR was carried out using gene-specific primers (QuantiTect Primer Assays, Qiagen) for *CDH1* (E-cadherin) (QT00080143), *SNAI1* (Snail1) (QT00010010), *SNAI2* (Snail2) (QT00044128), *ZEB1* (QT00008555), *ZEB2* (QT00008554), *TWIST1* (QT00011956), *COL1A1* (QT00037793), *ACTA2* (α-SMA) (QT00088102), *COL3A1* (QT00058233), *FN1* (QT00038024), *VIM* (QT00095795), *GAPDH* (QT01192646) or *ACTB* (β-actin) (QT01680476) with QuantiNova SYBR Green RT-PCR

kits (Qiagen). Relative transcript levels of target genes were normalised to *GAPDH* or *ACTB* (β-actin).

Immunofluorescence microscopy. Cells were fixed in 4% PBS-paraformaldehyde for 15 min, incubated in 0.1% Triton X-100 for 5 min on ice, then in 0.2% fish skin gelatine in PBS for 1 h and stained for 1 h with an anti-E-cadherin (1:100, BD Biosciences, 610182) or anti-p62/SQSTM1 (1:100, BD Biosciences, 610833) or anti-Snail2 (1:100, Cell Signalling Technology, 9585), p65/RELA (1:100, Cell Signalling Technology, 8242). Protein expression was detected using Alexa Fluor (1:400, Molecular Probes) for 20 min. DAPI or TO-PRO-3 (Invitrogen) was used to stain nuclei (1:1,000). Rhodamine phalloidin was used to visualize filamentous actin (F-actin) (Molecular Probes). For immunofluorescence staining of 3D cultures from ATII cells, spheres were fixed with 4% PBS-paraformaldehyde for 40 min, permeabilised in 0.5% Triton X-100 for 10 min on ice and stained with rhodamine phalloidin for 1 h at room temperature. Spheres were counterstained with DAPI. Samples were observed using a confocal microscope system (Leica SP8). Acquired images were analysed using Photoshop (Adobe Systems) according to the guidelines of the journal.

Wound-healing migration assay. The wound-healing migration assays were done in conjunction with siRNA transfections in ATII cells. 72 hours after siRNA transfections, confluent monolayers of cells were wounded with a p20 pipette tip (time 0). Phase-contrast images were taken using an Olympus inverted microscope at time 0 hour or 20 hours after the scratch wound, invasive cells were evaluated by ImageJ software (National Institutes of Health).

Transwell migration and Matrigel invasion assay. For the Transwell migration assay, Transwell membranes (8-μm pore size, 6.5-mm diameter; Corning Costar, 3422) were used.

The bottom chambers of the Transwell were filled with migration-inducing medium (with 50% fetal bovine serum). The top chambers were seeded with 1.5×10^5 live serum-starved control or *ATG5*-depleted ATII cells per well. After 24 h, the filters were fixed with 4% paraformaldehyde for 10 min at room temperature; subsequently, the cells on the upper side of the membrane were scraped with a cotton swab. Similar inserts coated with Matrigel (Corning, 354480) were used to determine invasive potential in invasion assays. Filters were stained with crystal violet for light microscopy. Images were taken using an Olympus inverted microscope and migratory cells were evaluated by ImageJ 1.42q software (National Institutes of Health).

Immunohistochemistry, haematoxylin and eosin (H/E) and tinctorial stains. Control or IPF lung tissues were fixed and embedded in paraffin wax; tissue sections (4μm) were processed and stained as previously described[18]. Briefly, the tissue sections were de-waxed, rehydrated and incubated with 3% hydrogen peroxide in methanol for 10 min to block endogenous peroxidase activity. Sections were then blocked with normal goat serum and incubated at room temperature with a primary antibody against p62/SQSTM1 (1:100, Progen, GP62_C), followed by a biotinylated secondary antibody (1:500, Vector Laboratories Ltd, UK); antibody binding was detected using streptavidin-conjugated horse-radish peroxidase and visualised using DAB (DAKO) before counterstaining with Mayer's Haematoxylin. For H/E stain, Shandon Varistain 24-4 automatic slide stainer (Thermo Fisher Scientific) was used. For tinctorial stain, Trichrome stain (Abcam ab150686) was used according to the manufacturers' instructions. Images were acquired using an Olympus Dotslide Scanner VS110.

Statistical analysis and repeatability of experiments. Each experiment was repeated at least twice. Unless otherwise noted, data are presented as mean and s.d., and a two-tailed, unpaired or paired Student's *t*-test was used to compare two groups for independent samples. $P < 0.05$ was considered statistically significant.

Acknowledgements

This project was supported by an Academy of Medical Sciences/the Wellcome Trust Springboard Award [SBF002\1038], the Wessex Medical Trust and AAIR Charity. CH was supported by Gerald Kerkut Charitable Trust and University of Southampton Central VC Scholarship Scheme. FC was supported by Medical Research Foundation [MRF-091-0003-RG-CONFO]. LY was supported by China Scholarship Council. YZ was supported by an Institute for Life Sciences PhD Studentship. JD was supported by the Francis Crick Institute which receives its core funding from Cancer Research UK (FC001070), the UK Medical Research Council (FC001070), and the Wellcome Trust (FC001070). XL was supported by the Ludwig Institute for Cancer Research. MGJ was supported by the Wellcome Trust [100638/Z/12/Z]. We thank Carine Fixmer, Maria Lane, Benjamin Johnson and the nurses of the Southampton Biomedical Research Unit for their help in the collection of human samples, supported by the Wessex Clinical Research Network and the National Institute of Health Research, UK.

Conflict of interest

The authors declare that they have no relevant conflict of interest.

References

1 Hutchinson J, Fogarty A, Hubbard R, McKeever T. Global incidence and mortality of idiopathic pulmonary fibrosis: a systematic review. *Eur Respir J* 2015; **46**(3): 795–806.

2 Richeldi L, Collard HR, Jones MG. Idiopathic pulmonary fibrosis. *Lancet* 2017; **389**(10082): 1941–1952.

3 Raghu G, Weycker D, Edelsberg J, Bradford WZ, Oster G. Incidence and Prevalence of Idiopathic Pulmonary Fibrosis. *Am J Respir Crit Care Med* 2006; **174**(7): 810–816.

4 Martinez-Lopez N, Athonvarangkul D, Singh R. Autophagy and aging. *Adv Exp Med Biol* 2015; **847**: 73–87.

5 Romero Y *et al.* mTORC1 activation decreases autophagy in aging and idiopathic pulmonary fibrosis and contributes to apoptosis resistance in IPF fibroblasts. *Aging Cell* 2016; **15**(6): 1103–1112.

6 Patel AS *et al.* Autophagy in Idiopathic Pulmonary Fibrosis. *PLoS One* 2012; **7**(7): e41394.

7 Rangarajan S *et al.* Novel Mechanisms for the Antifibrotic Action of Nintedanib. *Am J Respir Cell Mol Biol* 2016; **54**(1): 51–59.

8 Araya J *et al.* Insufficient autophagy in idiopathic pulmonary fibrosis. *Am J Physiol - Lung Cell Mol Physiol* 2013; **304**(1): L56–L69.

9 Ghavami S *et al.* Autophagy and the unfolded protein response promote profibrotic effects of TGF-β_1 in human lung fibroblasts. *Am J Physiol Cell Mol Physiol* 2018; **314**(3): L493–L504.

10 Bento CF *et al.* Mammalian Autophagy: How Does It Work? *Annu Rev Biochem* 2016; **85**(1): 685–713.

11 Singh KK *et al.* The Essential Autophagy Gene ATG7 Modulates Organ Fibrosis via

Regulation of Endothelial-to-Mesenchymal Transition. *J Biol Chem* 2015; **290**(5): 2547–2559.

12 Nieto A, Huang R, Jackson R, Thiery J. EMT: 2016. *Cell* 2016; **166**(1): 21–45.

13 Peinado H, Olmeda D, Cano A. Snail, Zeb and bHLH factors in tumour progression: an alliance against the epithelial phenotype? *Nat Rev Cancer* 2007; **7**(6): 415–428.

14 Nieto MA. The Ins and Outs of the Epithelial to Mesenchymal Transition in Health and Disease. *Annu Rev Cell Dev Biol* 2011; **27**(1): 347–376.

15 Rusten TE, Stenmark H. p62, an autophagy hero or culprit? *Nat Cell Biol* 2010; **12**(3): 207–209.

16 Xu Y *et al.* Single-cell RNA sequencing identifies diverse roles of epithelial cells in idiopathic pulmonary fibrosis. *JCI Insight* 2017; **1**(20): e90558.

17 Moscat J, Diaz-Meco MT. p62 at the crossroads of autophagy, apoptosis, and cancer. *Cell* 2009; **137**(6): 1001–4.

18 Yao L *et al.* Paracrine signalling during ZEB1-mediated epithelial–mesenchymal transition augments local myofibroblast differentiation in lung fibrosis. *Cell Death Differ* 2018; **26**(5): 1–15.

19 Molina-Arcas M, Hancock DC, Sheridan C, Kumar MS, Downward J. Coordinate Direct Input of Both KRAS and IGF1 Receptor to Activation of PI3 kinase in *KRAS* -Mutant Lung Cancer. *Cancer Discov* 2013; **3**(5): 548–563.

20 Coelho MA *et al.* Oncogenic RAS Signaling Promotes Tumor Immunoresistance by Stabilizing PD-L1 mRNA. *Immunity* 2017; **47**(6): 1083-1099.e6.

21 DeVorkin L, Lum JJ. Strategies to Block Autophagy in Tumor Cells. In: *Autophagy: Cancer, Other Pathologies, Inflammation, Immunity, Infection, and Aging*. Academic Press, 2014, pp 121–130.

22 Thiery JP, Sleeman JP. Complex networks orchestrate epithelial–mesenchymal

transitions. *Nat Rev Mol Cell Biol* 2006; **7**(2): 131–142.

23 Ballou LM, Lin RZ. Rapamycin and mTOR kinase inhibitors. *J Chem Biol* 2008; **1**(1–4): 27–36.

24 Wang Y *et al.* Autophagy inhibition specifically promotes epithelial-mesenchymal transition and invasion in RAS-mutated cancer cells. *Autophagy* 2019; : 1–14.

25 Thannickal VJ, Zhou Y, Gaggar A, Duncan SR. Fibrosis: ultimate and proximate causes. *J Clin Invest* 2014; **124**(11): 4673–4677.

26 Wynn TA. Fibrotic disease and the T(H)1/T(H)2 paradigm. *Nat Rev Immunol* 2004; **4**(8): 583–94.

27 Wynn TA, Ramalingam TR. Mechanisms of fibrosis: therapeutic translation for fibrotic disease. *Nat Med* 2012; **18**(7): 1028–1040.

28 Pardo A, Selman M. Lung Fibroblasts, Aging, and Idiopathic Pulmonary Fibrosis. *Ann Am Thorac Soc* 2016; **13**(Supplement_5): S417–S421.

29 Raghu G *et al.* Diagnosis of Idiopathic Pulmonary Fibrosis. An Official ATS/ERS/JRS/ALAT Clinical Practice Guideline. *Am J Respir Crit Care Med* 2018; **198**(5): e44–e68.

30 Minagawa S *et al.* Accelerated epithelial cell senescence in IPF and the inhibitory role of SIRT6 in TGF-β-induced senescence of human bronchial epithelial cells. *Am J Physiol Cell Mol Physiol* 2011; **300**(3): L391–L401.

31 Tsakiri KD *et al.* Adult-onset pulmonary fibrosis caused by mutations in telomerase. *Proc Natl Acad Sci U S A* 2007; **104**(18): 7552–7.

32 Alder JK *et al.* Short telomeres are a risk factor for idiopathic pulmonary fibrosis. *Proc Natl Acad Sci U S A* 2008; **105**(35): 13051–6.

33 Bueno M *et al.* PINK1 deficiency impairs mitochondrial homeostasis and promotes lung fibrosis. *J Clin Invest* 2015; **125**(2): 521–538.

34 Fingerlin TE *et al.* Genome-wide association study identifies multiple susceptibility loci for pulmonary fibrosis. *Nat Genet* 2013; **45**(6): 613–20.

35 Spagnolo P, Tzouvelekis A, Bonella F. The Management of Patients With Idiopathic Pulmonary Fibrosis. *Front Med* 2018; **5**: 148.

36 Hill C, Jones MG, Davies DE, Wang Y. Epithelial-Mesenchymal Transition Contributes to Pulmonary Fibrosis via Aberrant Epithelial/Fibroblastic Cross-Talk. *J Lung Heal Dis* 2019; **3**(2): 31–35.

37 Chilosi M *et al.* Epithelial to mesenchymal transition-related proteins ZEB1, β-catenin and β-tubulin-III in idiopathic pulmonary fibrosis. *Mod Pathol* 2017; **30**(1): 26–38.

38 Park JS *et al.* Clinical significance of mTOR, ZEB1, ROCK1 expression in lung tissues of pulmonary fibrosis patients. *BMC Pulm Med* 2014; **14**(1): 168.

39 Lomas NJ, Watts KL, Akram KM, Forsyth NR, Spiteri MA. Idiopathic pulmonary fibrosis: immunohistochemical analysis provides fresh insights into lung tissue remodelling with implications for novel prognostic markers. *Int J Clin Exp Pathol* 2012; **5**(1): 58–71.

40 Willis BC *et al.* Induction of epithelial-mesenchymal transition in alveolar epithelial cells by transforming growth factor-beta1: potential role in idiopathic pulmonary fibrosis. *Am J Pathol* 2005; **166**(5): 1321–1332.

41 Harada T *et al.* Epithelial–mesenchymal transition in human lungs with usual interstitial pneumonia: Quantitative immunohistochemistry. *Pathol Int* 2010; **60**(1): 14–21.

42 Marmai C *et al.* Alveolar epithelial cells express mesenchymal proteins in patients with idiopathic pulmonary fibrosis. *AJP Lung Cell Mol Physiol* 2011; **301**(1): L71–L78.

43 Rock JR *et al.* Multiple stromal populations contribute to pulmonary fibrosis without

evidence for epithelial to mesenchymal transition. *Proc Natl Acad Sci* 2011; **108**(52): E1475–E1483.

44 Humphreys BD *et al.* Fate Tracing Reveals the Pericyte and Not Epithelial Origin of Myofibroblasts in Kidney Fibrosis. *Am J Pathol* 2010; **176**(1): 85–97.

45 Tanjore H *et al.* Contribution of Epithelial-derived Fibroblasts to Bleomycin-induced Lung Fibrosis. *Am J Respir Crit Care Med* 2009; **180**(7): 657–665.

46 Degryse AL *et al.* TGFβ signaling in lung epithelium regulates bleomycin-induced alveolar injury and fibroblast recruitment. *Am J Physiol Lung Cell Mol Physiol* 2011; **300**(6): L887-97.

47 Grande MT *et al.* Snail1-induced partial epithelial-to-mesenchymal transition drives renal fibrosis in mice and can be targeted to reverse established disease. *Nat Med* 2015; **21**(9): 989–997.

48 Lovisa S *et al.* Epithelial-to-mesenchymal transition induces cell cycle arrest and parenchymal damage in renal fibrosis. *Nat Med* 2015; **21**(9): 998–1009.

49 Harris H, Rubinsztein DC. Control of autophagy as a therapy for neurodegenerative disease. *Nat Rev Neurol* 2012; **8**(2): 108–117.

50 White E. Deconvoluting the context-dependent role for autophagy in cancer. *Nat Rev Cancer* 2012; **12**(6): 401–410.

51 Saha S, Panigrahi DP, Patil S, Bhutia SK. Autophagy in health and disease: A comprehensive review. *Biomed Pharmacother* 2018; **104**: 485–495.

52 Rubinsztein DC, Mariño G, Kroemer G. Autophagy and Aging. *Cell* 2011; **146**(5): 682–695.

53 Lamouille S, Xu J, Derynck R. Molecular mechanisms of epithelial–mesenchymal transition. *Nat Rev Mol Cell Biol* 2014; **15**(3): 178–196.

54 Jayachandran A *et al.* SNAI transcription factors mediate epithelial-mesenchymal

transition in lung fibrosis. *Thorax* 2009; **64**(12): 1053–61.

55 Catalano M *et al.* Autophagy induction impairs migration and invasion by reversing EMT in glioblastoma cells. *Mol Oncol* 2015; **9**(8): 1612–1625.

56 Wei R *et al.* FAT4 regulates the EMT and autophagy in colorectal cancer cells in part via the PI3K-AKT signaling axis. *J Exp Clin Cancer Res* 2019; **38**(1): 112.

57 Gugnoni M, Sancisi V, Manzotti G, Gandolfi G, Ciarrocchi A. Autophagy and epithelial–mesenchymal transition: an intricate interplay in cancer. *Cell Death Dis* 2016; **7**(12): e2520.

58 Sakata J *et al.* Inhibition of ZEB1 leads to inversion of metastatic characteristics and restoration of paclitaxel sensitivity of chronic chemoresistant ovarian carcinoma cells. *Oncotarget* 2017; **8**(59): 99482–99494.

59 Kothari A, Mi Z, Zapf M, Kuo P. Novel clinical therapeutics targeting the epithelial to mesenchymal transition. *Clin Transl Med* 2014; **3**: 35.

60 Conforti F *et al.* The histone deacetylase inhibitor, romidepsin, as a potential treatment for pulmonary fibrosis. *Oncotarget* 2017; **8**(30): 48737–48754.

61 Jones MG *et al.* Nanoscale dysregulation of collagen structure-function disrupts mechano-homeostasis and mediates pulmonary fibrosis. *Elife* 2018; **7**: e36354.

62 Yu W *et al.* Formation of Cysts by Alveolar Type II Cells in Three-dimensional Culture Reveals a Novel Mechanism for Epithelial Morphogenesis. *Mol Biol Cell* 2007; **18**(5): 1693–1700.

Figure Legends

Figure 1 p62/SQSTM1 is highly expressed in IPF fibroblastic foci and epithelial cells of thickened alveoli septae where collagen deposition in the interstitium is also evident. Serial sections of IPF (fibroblastic foci in **a**, and epithelial cells of thickened alveoli septae in **b**) or control lung tissue (**c**) were stained for p62/SQSTM1 (top panel), with H&E (middle panel) or Masson's trichrome stain (bottom panel, collagen shown in blue). $n = 3$. * a fibroblastic focus. Scale bars: 50 μm.

Figure 2 Autophagic activity altered by chemicals affects cellular plasticity of ATII cells. (**a**) Protein expression of E-Cadherin, Snail2, p62/SQSTM1 and LC3 in ATII cells treated with HCQ (25 μM) at indicated times. β-actin was used as a loading control. (**b**) Fold change in mRNA levels of *CDH1* (E-cadherin), *VIM* (Vimentin), *SNAI1* (Snail1), *SNAI2* (Snail2), *TWIST1*, *ZEB1* and *ZEB2* in ATII cells cultured in the absence or presence of HCQ (μM) for 24 hrs. GAPDH-normalised mRNA levels in control cells were used to set the baseline value at unity. Data are mean ± s.d. $n = 3$ samples per group. *** $P < 0.001$. (**c**) Immunofluorescence staining of Snail2 (green) and F-actin (red) in ATII cells cultured in the absence or presence of HCQ (25 μM) for 24 hrs. Rhodamine-phalloidin was used to stain F-actin. DAPI (blue) was used to stain nuclei. Scale bar: 40μm.

Figure 3 Autophagy inhibition by *ATG5* depletion induces EMT and cell migration in ATII cells. (**a**) Protein expression of E-cadherin, p62/SQSTM and ATG12–ATG5 in ATII cells transfected with indicated siRNAs. β-tubulin was used as a loading control. (**b**) Fold change in the mRNA level of *CDH1* (E-cadherin) in ATII cells transfected with indicated siRNAs. GAPDH-normalised mRNA levels in control cells were used to set the baseline value at unity. Data are mean ± s.d. $n = 3$ samples per group. ** $P < 0.01$. (**c**) Immunofluorescence

staining of p62/SQSTM (green) and F-actin (red) in ATII cells transfected with control or *ATG5* siRNAs. Rhodamine-phalloidin was used to stain F-actin. DAPI (blue) was used to stain nuclei. Scale bar: 40 μm. (**d**) Scratch wound assay of ATII cells transfected with control or *ATG5* siRNAs. Representative images of ATII cells with the indicated treatments at time 0 or 20 hrs after the scratch wound. Wounds have been artificially coloured red to aid visualization. Scale bar: 200 μm. The graph shows the area of a wound evaluated with ImageJ, and data are mean ± s.d. $n = 3$. *** $P < 0.001$. (**e**) Transwell migration assays in control or *ATG5*-depleted ATII cells. Cells were stained with crystal violet. Scale bar: 100 μm. Data are mean ± s.d. $n = 3$. *** $P < 0.001$.

Figure 4 Autophagy inhibition induces EMT via p62/SQSTM1-NF-κB-Snail2 pathway in ATII cells. (**a**) Immunofluorescence staining of p62/SQSTM1 (red) and p65/RELA (green) in ATII cells treated with hydroxychloroquine (HCQ, 25 μM) for 24 hrs. DAPI (blue) was used to stain nuclei. Scale bar: 40 μm. (**b**) Protein expression of Snail2, p65/RELA and p62/SQSTM1 in ATII cells transfected with the indicated siRNAs followed by treatment of HCQ (25 μM) for 24 hrs. For protein expression of p62/SQSTM1, both short and long exposures (respectively) are shown. β-tubulin was used as a loading control.

Figure 5 ATII cells undergoing autophagy inhibition-induced EMT induce fibroblast activation via Snail2-regulated paracrine signalling. (**a)** Protein expression of E-cadherin, ATG12–ATG5 and Snail2 in ATII cells transfected with indicated siRNAs. β-tubulin was used as a loading control. (**b** and **c**) Protein expression of α-SMA and phospho-Smad2 (p-Smad2) in IPFFs with indicated treatments. β-tubulin was used as a loading control. Scores under the bands are relative levels when compared with indicated controls (1.0). The graphs

show relative α-SMA protein levels evaluated with ImageJ, and data are mean ± s.d. $n = 3$. * $P < 0.05$. *** $P < 0.001$.

Figure 6 Autophagy inhibition-mediated epithelial-mesenchymal transition augments local myofibroblast differentiation in pulmonary fibrosis. Diagrams showing autophagy inhibition induces EMT via p62/SQSMT1-NFκB-Snail2 pathway in alveolar epithelial cells (**a**) and local micro-injuries to ageing alveolar epithelium causes persistent activation of alveolar epithelial cells, which secrete numerous profibrogenic factors, driving local myofibroblast differentiation (**b**).

Figure 1

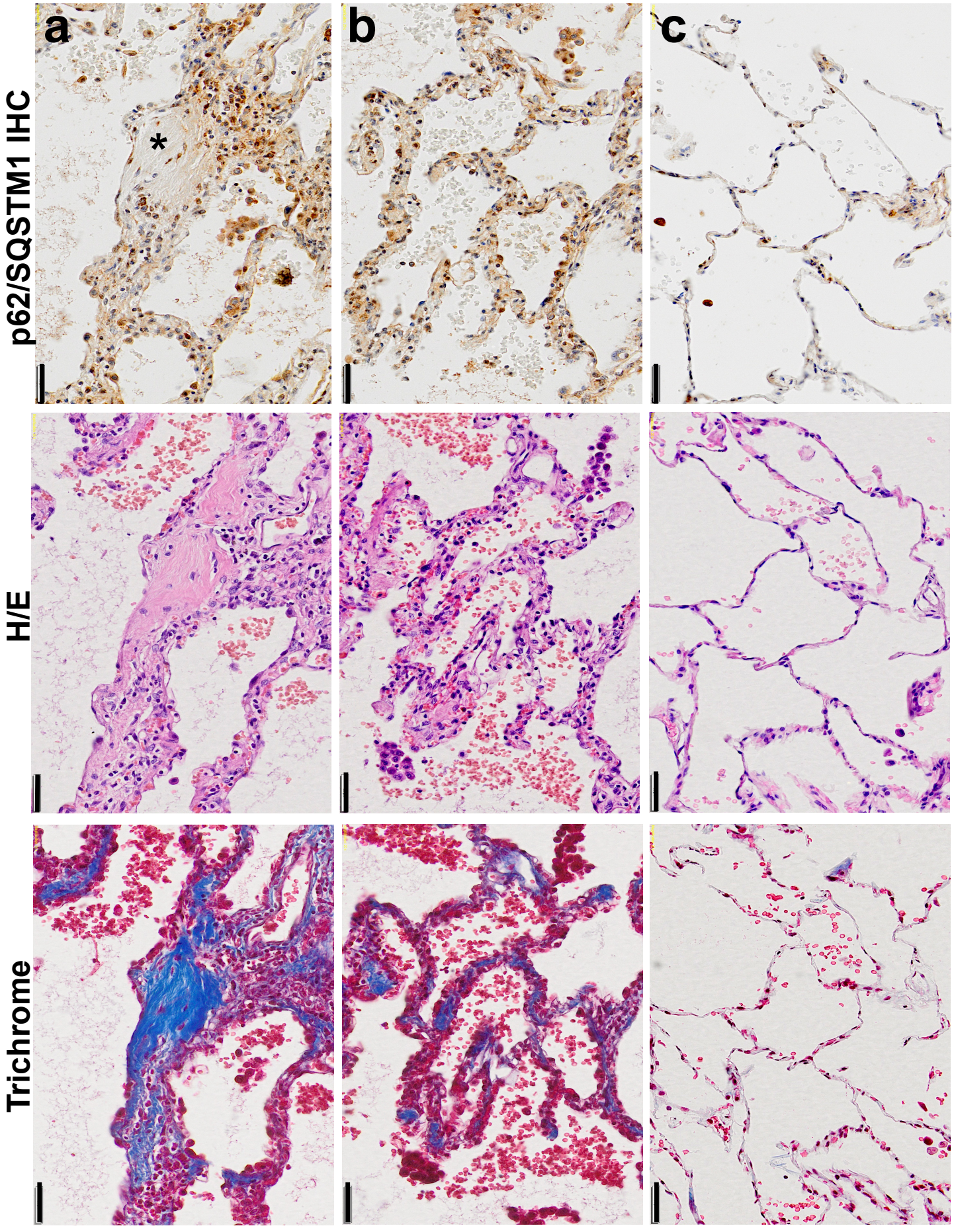

Figure 2

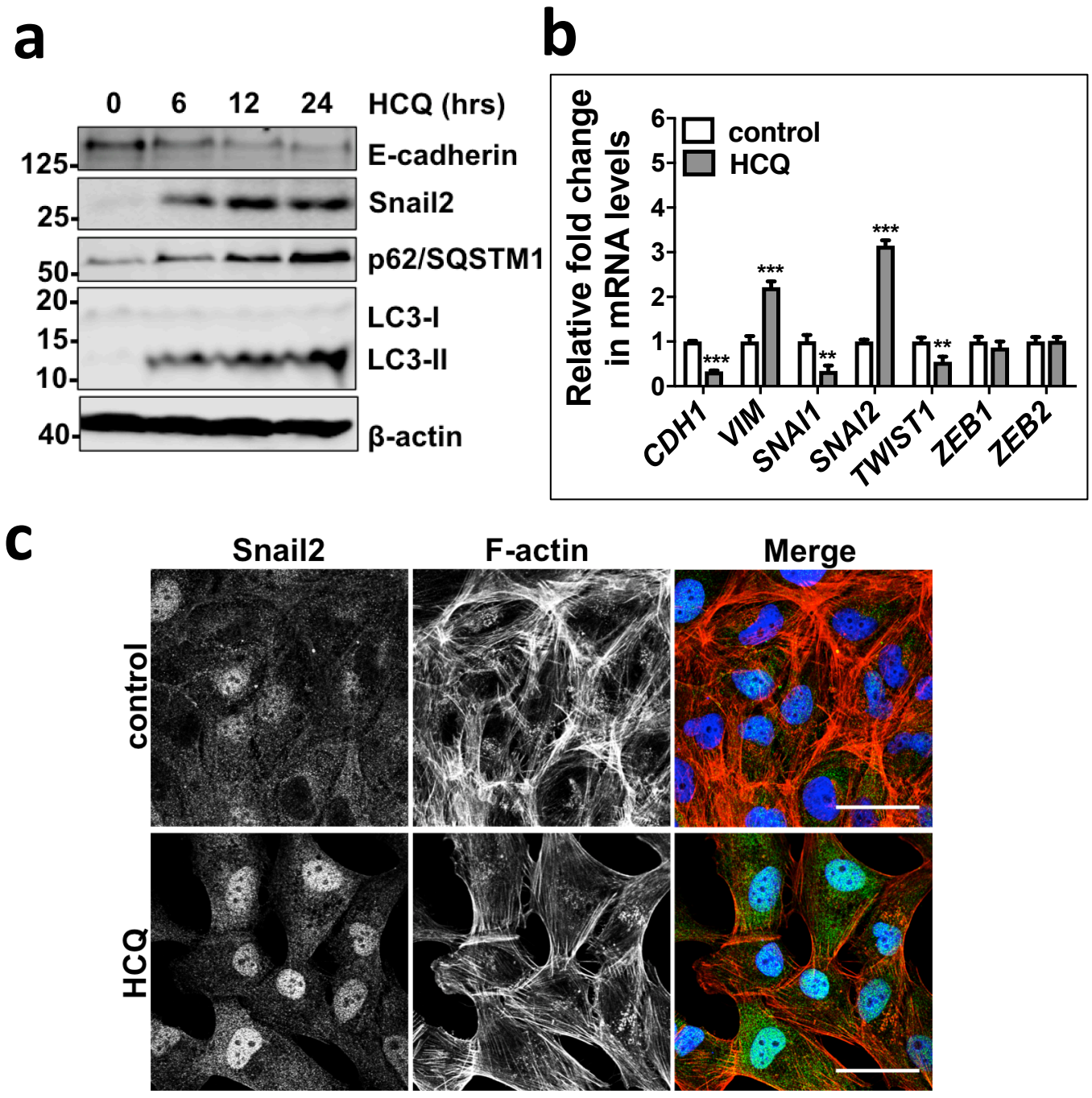
a
0
6
12
24
HCQ (hrs)
125
E-cadherin
25
Snail2
50
p62/SQSTM1
20
15
10
LC3-I
LC3-II
40
β-actin
b
Relative fold change in mRNA levels
control
HCQ
6
5
4
3
2
1
0
***
***
**
***
**
CDH1
VIM
SNAI1
SNAI2
TWIST1
ZEB1
ZEB2
c
Snail2
F-actin
Merge
control
HCQ

Figure 3

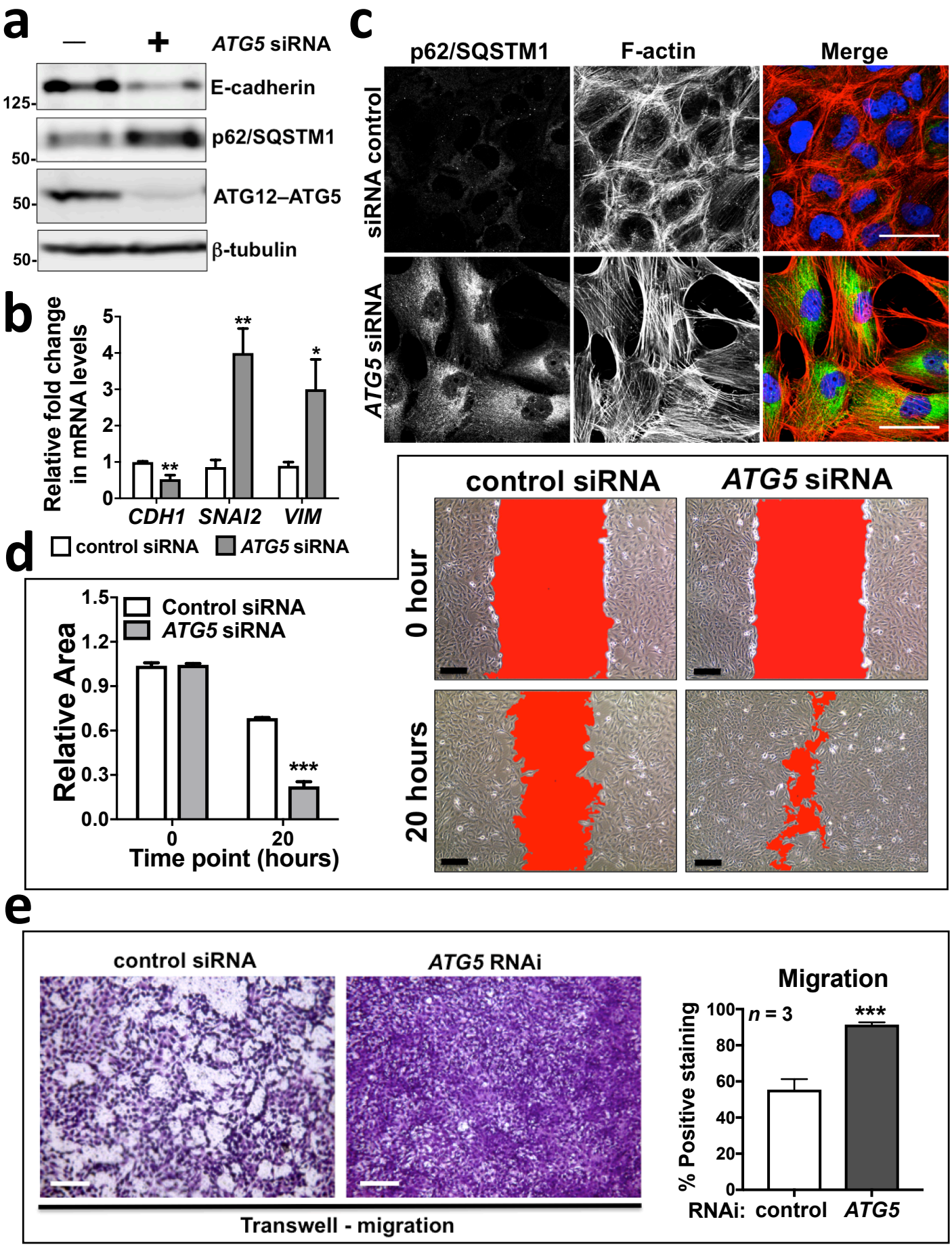
a
—
+
ATG5 siRNA
125-
E-cadherin
p62/SQSTM1
50-
50-
ATG12–ATG5
50-
β-tubulin
b
Relative fold change in mRNA levels
5
4
3
2
1
0
**
**
*
CDH1
SNAI2
VIM
control siRNA
ATG5 siRNA
c
p62/SQSTM1
F-actin
Merge
siRNA control
ATG5 siRNA
d
control siRNA
ATG5 siRNA
0 hour
20 hours
Relative Area
1.5
1.2
0.9
0.6
0.3
0.0
Control siRNA
ATG5 siRNA
***
0
20
Time point (hours)
e
control siRNA
ATG5 RNAi
Transwell - migration
Migration
% Positive staining
100
80
60
40
20
0
n = 3
***
RNAi: control
ATG5

Figure 4

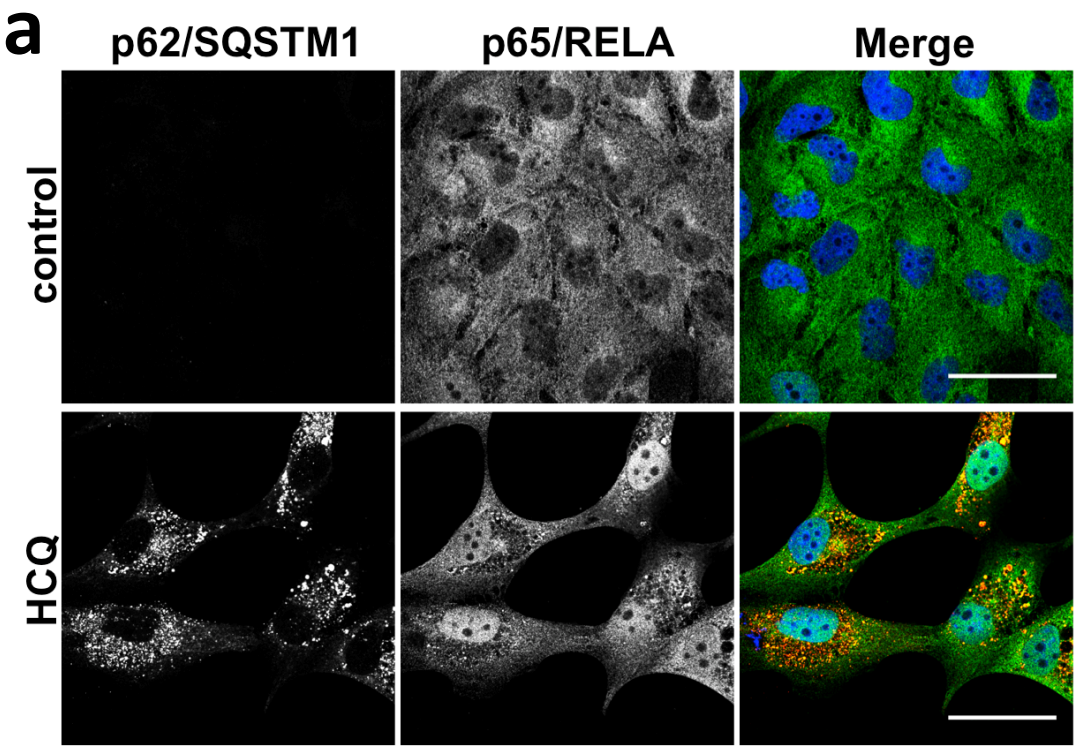
a
p62/SQSTM1
p65/RELA
Merge
control
HCQ

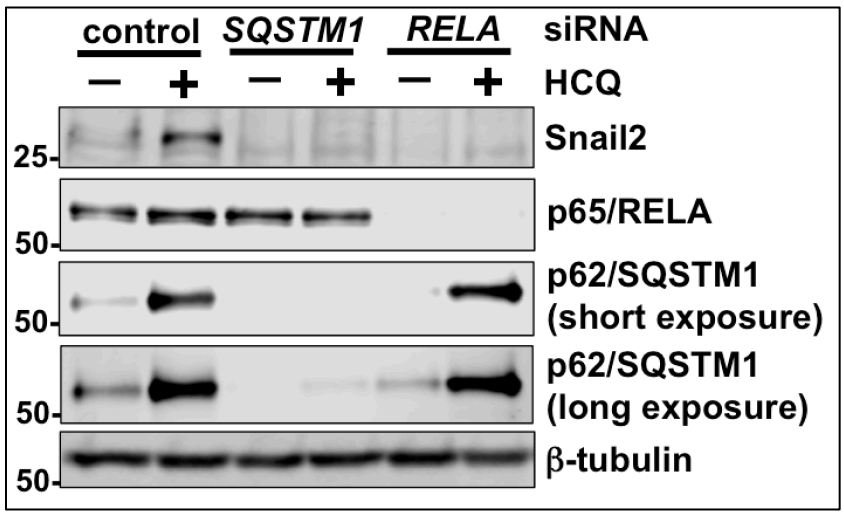
b
control
SQSTM1
RELA
siRNA
HCQ
Snail2
p65/RELA
p62/SQSTM1
(short exposure)
p62/SQSTM1
(long exposure)
β-tubulin
25
50
50
50
50

Figure 5

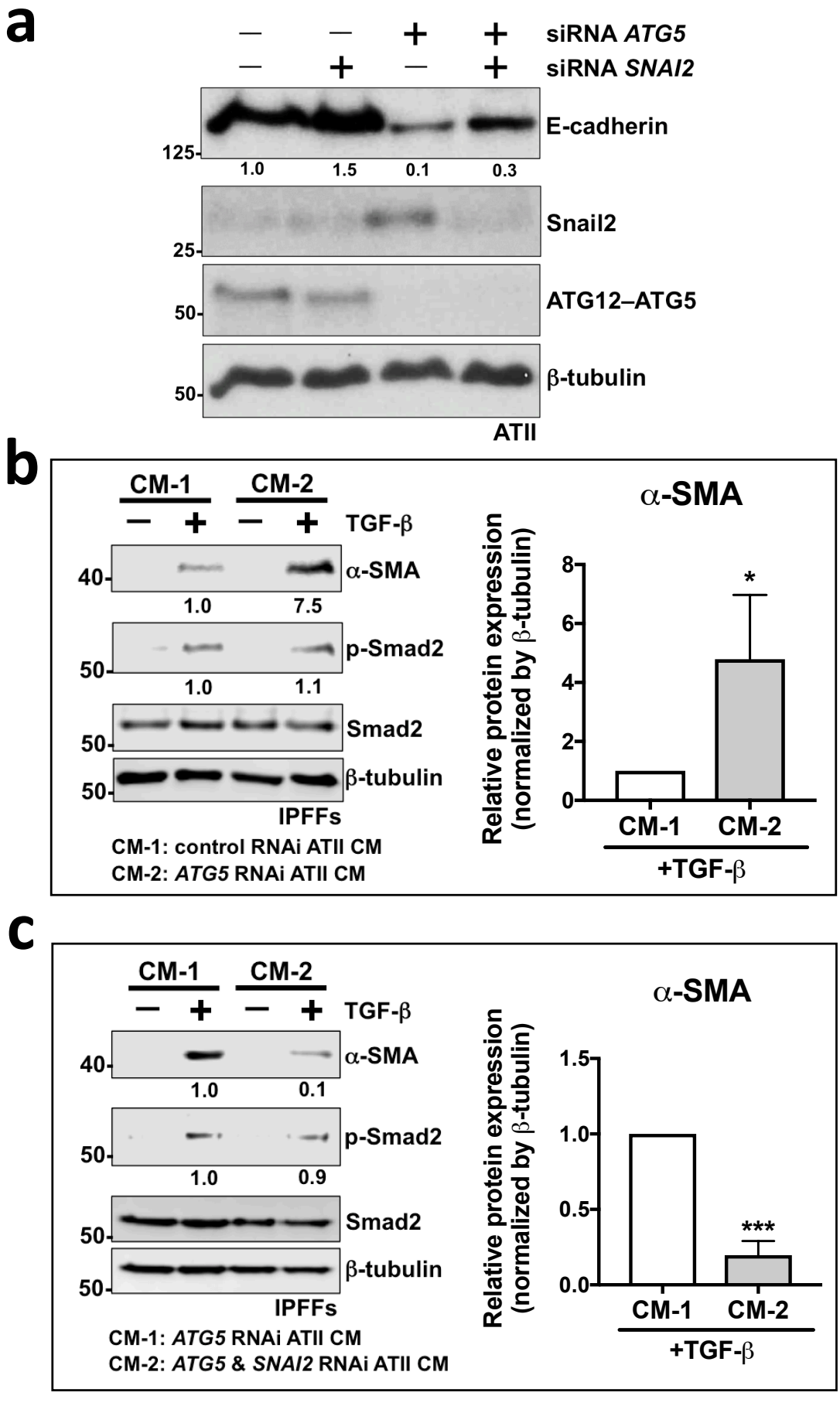
a
siRNA ATG5
siRNA SNAI2
E-cadherin
125
1.0
1.5
0.1
0.3
Snail2
25
ATG12–ATG5
50
β-tubulin
50
ATII
b
CM-1
CM-2
TGF-β
α-SMA
40
1.0
7.5
p-Smad2
50
1.0
1.1
Smad2
50
β-tubulin
50
IPFFs
CM-1: control RNAi ATII CM
CM-2: ATG5 RNAi ATII CM
α-SMA
Relative protein expression (normalized by β-tubulin)
8
6
4
2
0
*
CM-1
CM-2
+TGF-β
c
CM-1
CM-2
TGF-β
α-SMA
40
1.0
0.1
p-Smad2
50
1.0
0.9
Smad2
50
β-tubulin
50
IPFFs
CM-1: ATG5 RNAi ATII CM
CM-2: ATG5 & SNAI2 RNAi ATII CM
α-SMA
Relative protein expression (normalized by β-tubulin)
1.5
1.0
0.5
0.0
***
CM-1
CM-2
+TGF-β

Figure 6

a


Autophagy
p62/SQSTM1
NFκB
Snail2
EMT

b

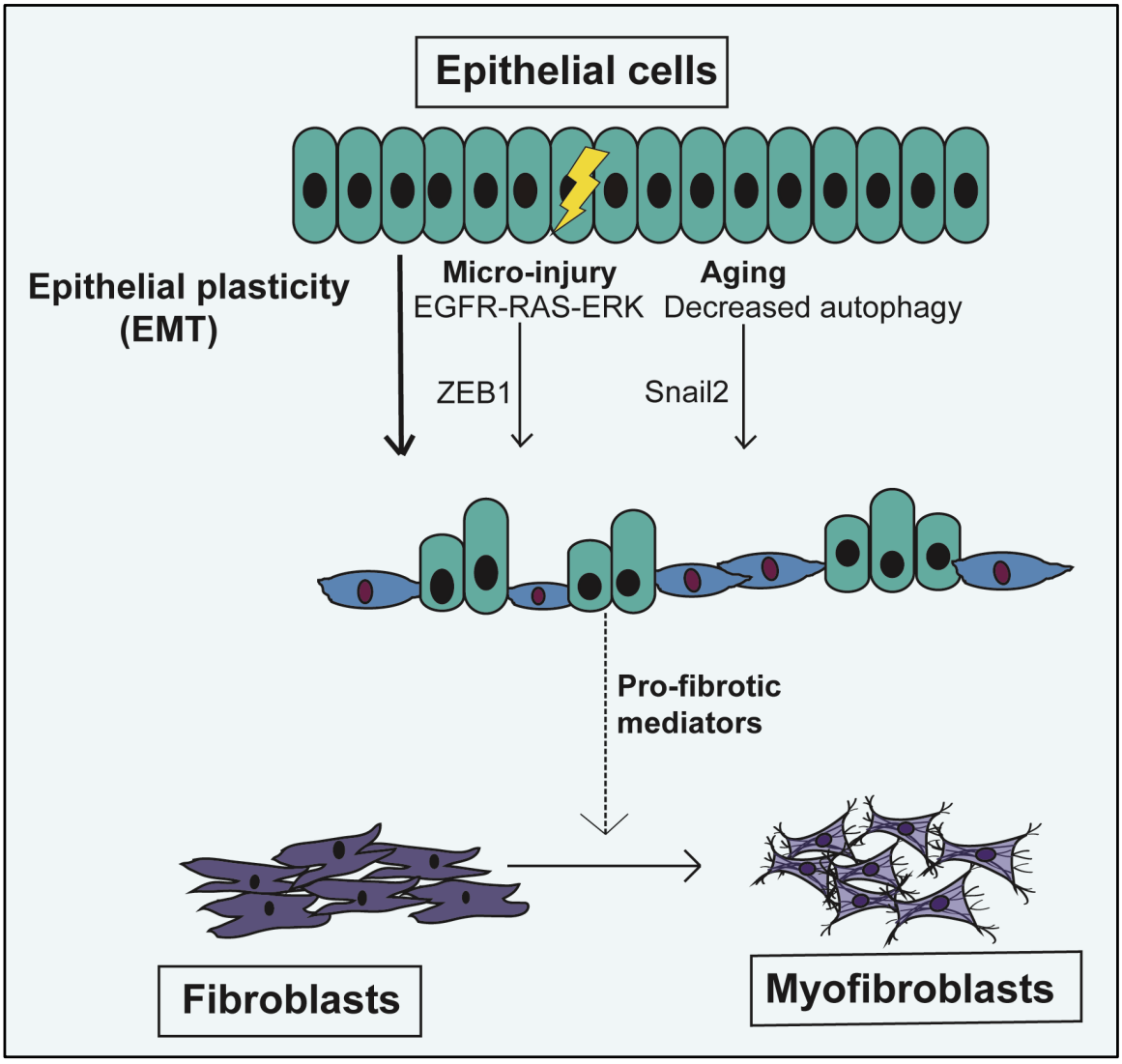
Epithelial cells
Epithelial plasticity (EMT)
Micro-injury
EGFR-RAS-ERK
Aging
Decreased autophagy
ZEB1
Snail2
Pro-fibrotic mediators
Fibroblasts
Myofibroblasts

Autophagy inhibition-mediated epithelial mesenchymal transition augments local myofibroblast differentiation in pulmonary fibrosis

Supplementary Figure Legends

Supplementary Figure 1 The protein level, but not the mRNA level, of p62/SQSTM1 is up regulated in IPF epithelial cells. **(a)** Sections from IPF or control lung tissues were stained for p62/SQSTM1. Scale bars: 50 μm. **(b)** Decreased mRNA levels of *SQSTM1* (p62) in IPF epithelial cells are shown by an online LGEA Web Portal (https://research.cchmc.org/pbge/lunggens/mainportal.html).

Supplementary Figure 2 Autophagy inhibition with Bafilomycin A1 (Baf-A1) induces EMT in ATII cells. (**a**) Protein expression of E-cadherin, p62/SQSTM1 and LC3 in ATII cells treated with Baf-A1 (10nM) for the indicated period. β-actin was used as a loading control. (**b**) Fold change in mRNA levels of *CDH1* (E-cadherin), *VIM* (Vimentin), *SNAI1* (Snail1), *SNAI2* (Snail2), *TWIST1*, *ZEB1* and *ZEB2* in ATII cells cultured in the absence or presence of Baf-A1 (10 nM) for 24 hrs. GAPDH-normalised mRNA levels in control cells were used to set the baseline value at unity. Data are mean ± s.d. $n = 3$ samples per group. ** $P < 0.01$. *** $P < 0.001$. (**c**) Representative 3D confocal images of ATII cells cultured in Matrigel in the absence or presence of Baf-A1 (10 nM) for 48 hrs. Spheres were stained for F-actin with Rhodamine-phalloidin (red) and DAPI (blue). Scale bars: 40μm.

Supplementary Figure 3 Autophagy inhibition by *ATG5* depletion in alveolar epithelial cells induces EMT and invasion. (**a**) Protein expression of E-cadherin, Snail2, ATG12–ATG5, LC3 and p62/SQSTM1 in A549 cells transfected with control or *ATG5* siRNA. β-

tubulin was used as a loading control. (**b**) Fold change in mRNA levels of *CDH1* (E-cadherin), *SNAI1* (Snail1), *SNAI2* (Snail2), *TWIST1*, *ZEB1* and *ZEB2* in A549 cells transfected with control or *ATG5* siRNA. GAPDH-normalised mRNA levels in control cells were used to set the baseline value at unity. Data are mean ± s.d. $n = 3$ samples per group. *** $P < 0.001$. (**c**) Immunofluorescence staining of p62/SQSTM1 (red) and E-cadherin (green) in A549 cells transfected with control or *ATG5* siRNA. Scale bar: 20 μm. (d) Transwell Matrigel invasion assays in control of *ATG5*-depleted ATII cells. Cells were stained with crystal violet. Data are mean ± s.d. $n = 3$. *** $P < 0.001$.

Supplementary Figure 4 Autophagic activity altered by Rapamycin affects cellular plasticity of ATII cells. (**a**) Protein expression of p62/SQSTM1, phospho-mTOR (p-mTOR), mTOR, ATG12–ATG5 and LC3 with indicated treatments in ATII cells. β-tubulin was used as a loading control. (**b)** Fold change in mRNA levels of *CDH1* (E-cadherin), *VIM* (Vimentin) and *SNAI2* (Snail2) in ATII cells with indicated treatments. β-actin normalised mRNA levels in control cells were used to set the baseline value at unity. Data are mean ± s.d. $n = 3$ samples per group. * $P < 0.05$. ** $P < 0.01$. *** $P < 0.001$.

Supplementary Figure 5 Autophagy inhibition induces EMT via p62/SQSTM1-NF-κB-Snail2 pathway in A549 cells. (**a**) Protein expression of ATG12–ATG5, p65/RELA and p62/SQSTM1 with indicated treatments in A549 cells. β-tubulin was used as a loading control. (**b)** Fold change in mRNA levels of *CDH1* (E-cadherin) or *SNAI2* (Snail2) in A549 cells with indicated treatments. GAPDH-normalised mRNA levels in control cells were used to set the baseline value at unity. Data are mean ± s.d. $n = 3$ samples per group. *** $P < 0.001$.

Supplementary Figure 6 ATII cells undergoing autophagy inhibition-induced EMT induce fibroblast activation via Snail2-regulated paracrine signalling. Fold change in mRNA levels of *COL1A1*, *COL3A1*, *FN1* and *ACTA2* in ATII cells transfected with the indicated siRNA. β-actin-normalised mRNA levels in control. Data are mean ± s.d. $n = 3$ samples per group. ** $P < 0.01$. *** $P < 0.001$.

Supplementary Figure 1

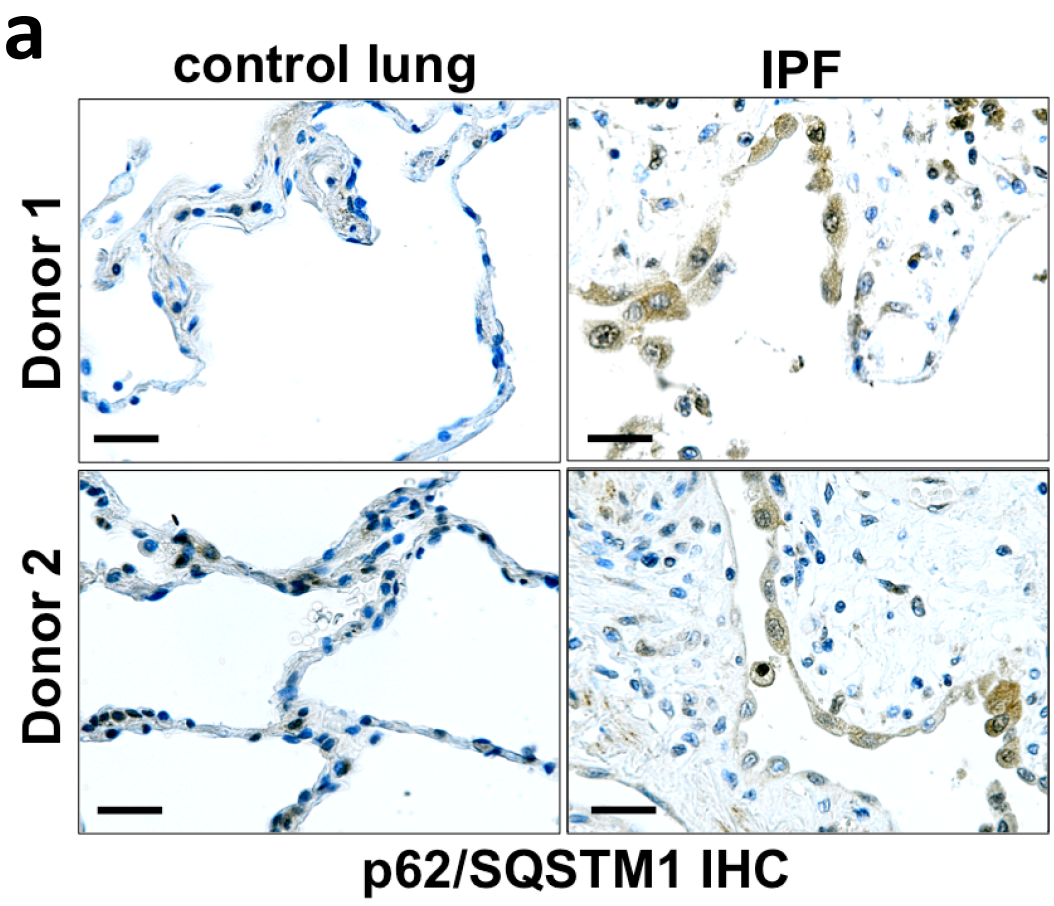

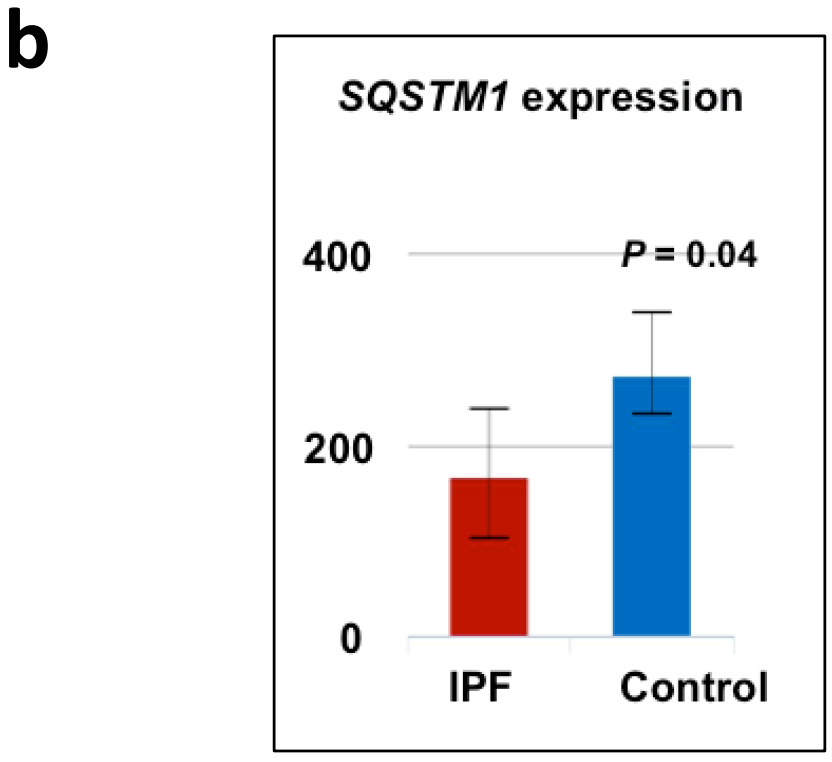

Supplementary Figure 2

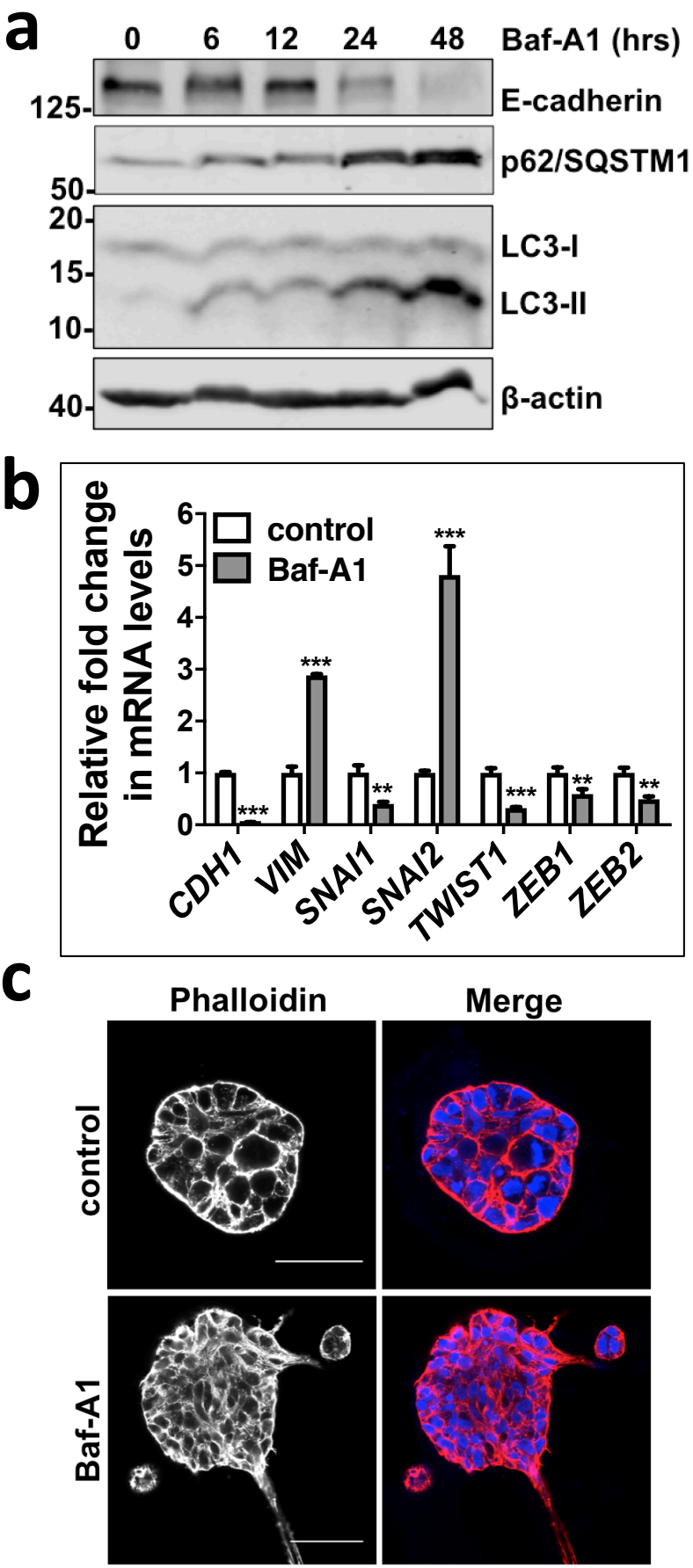

Supplementary Figure 3

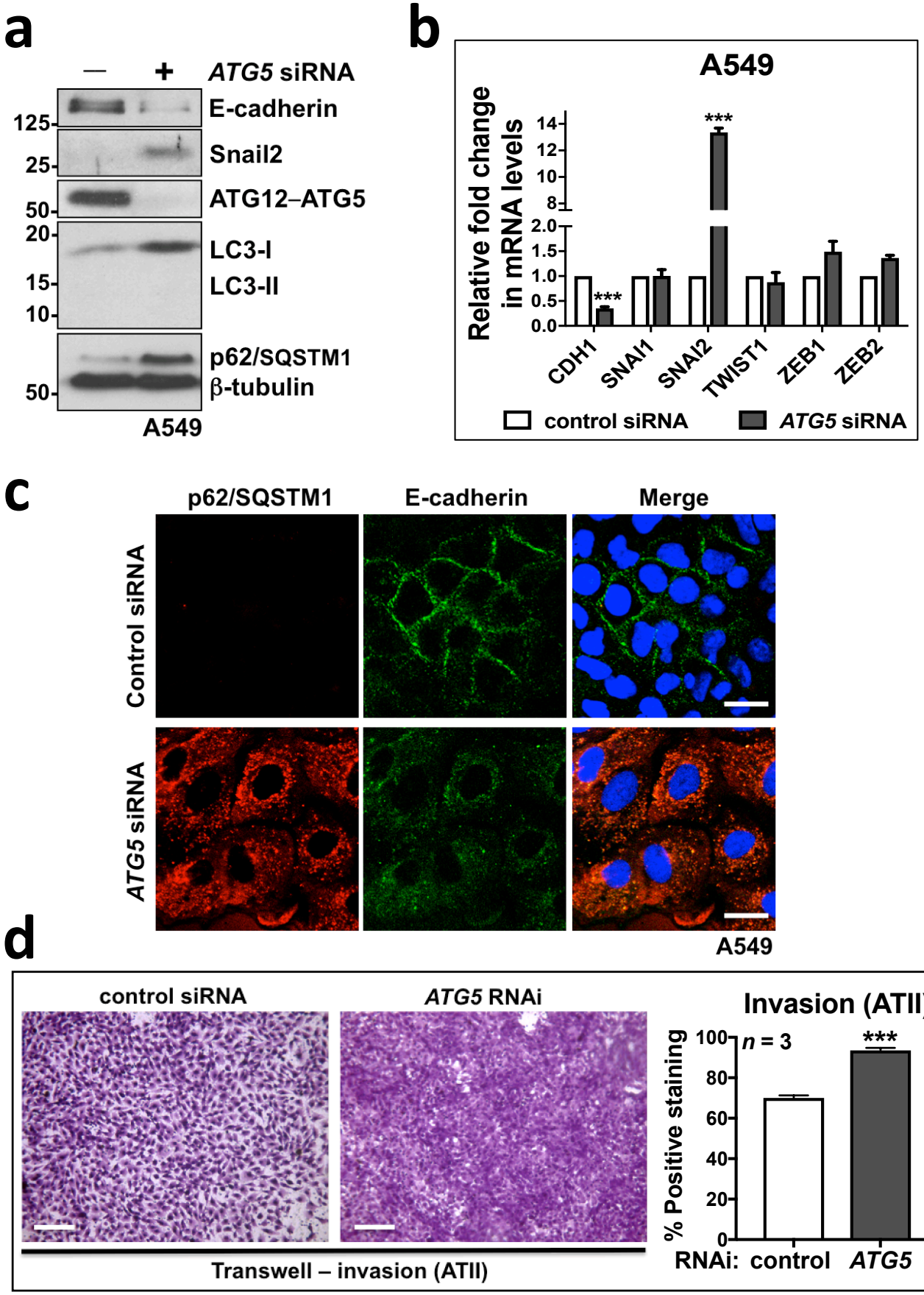

Supplementary Figure 4

a

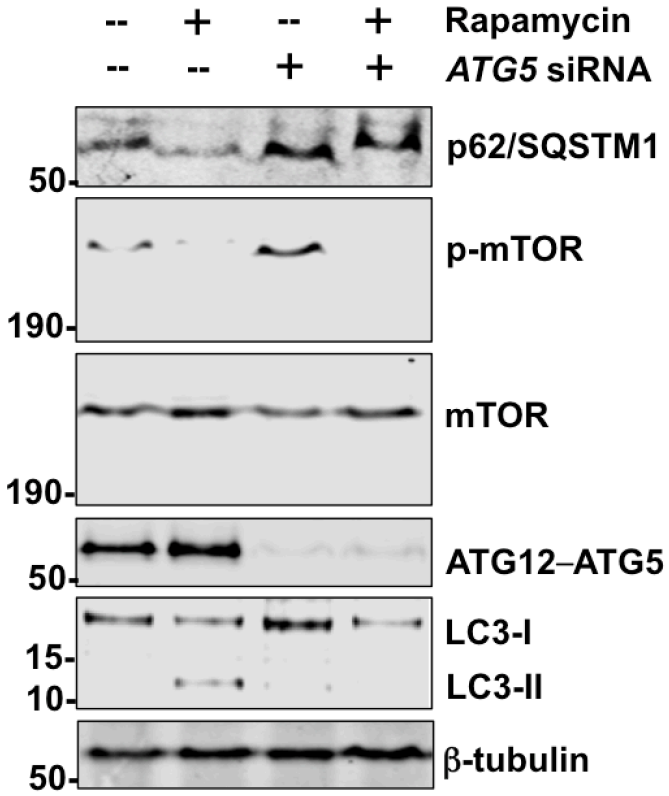

b

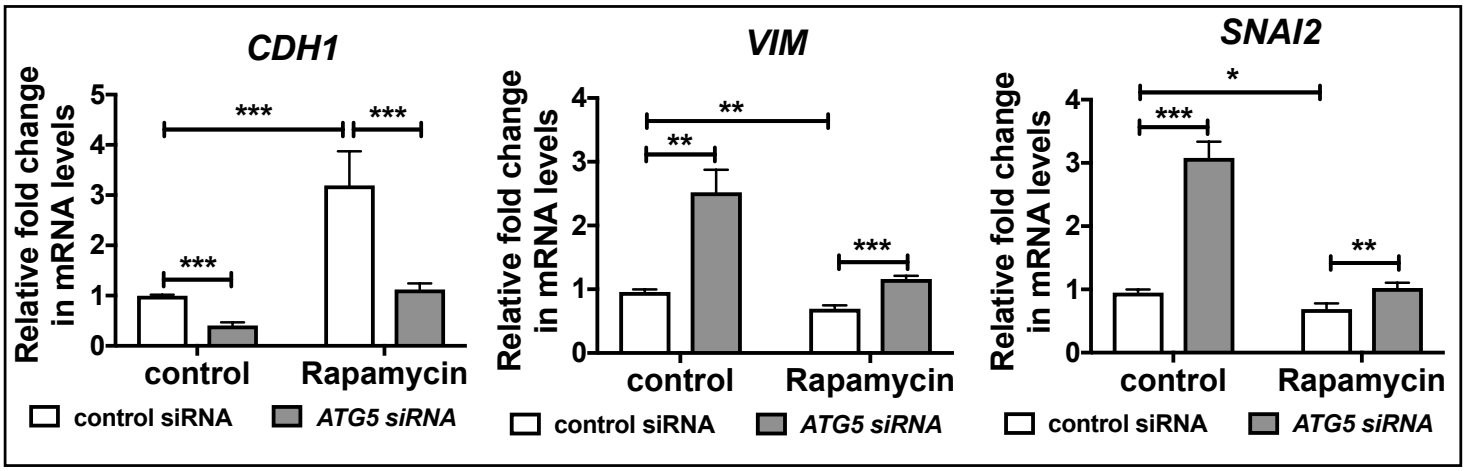

Supplementary Figure 5

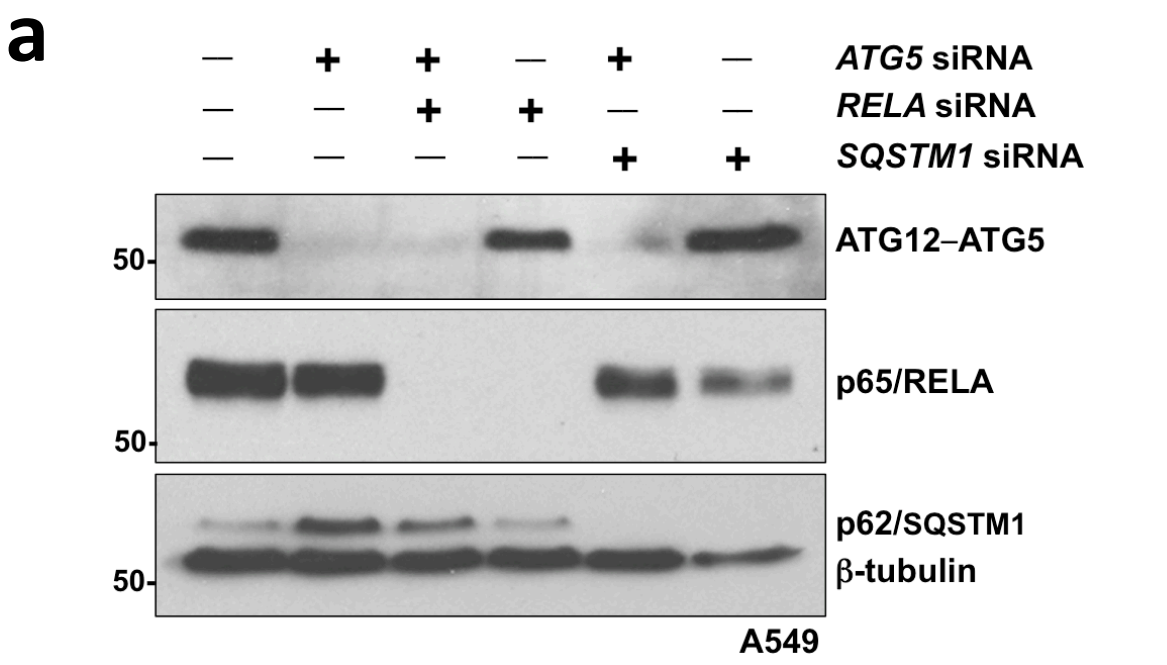

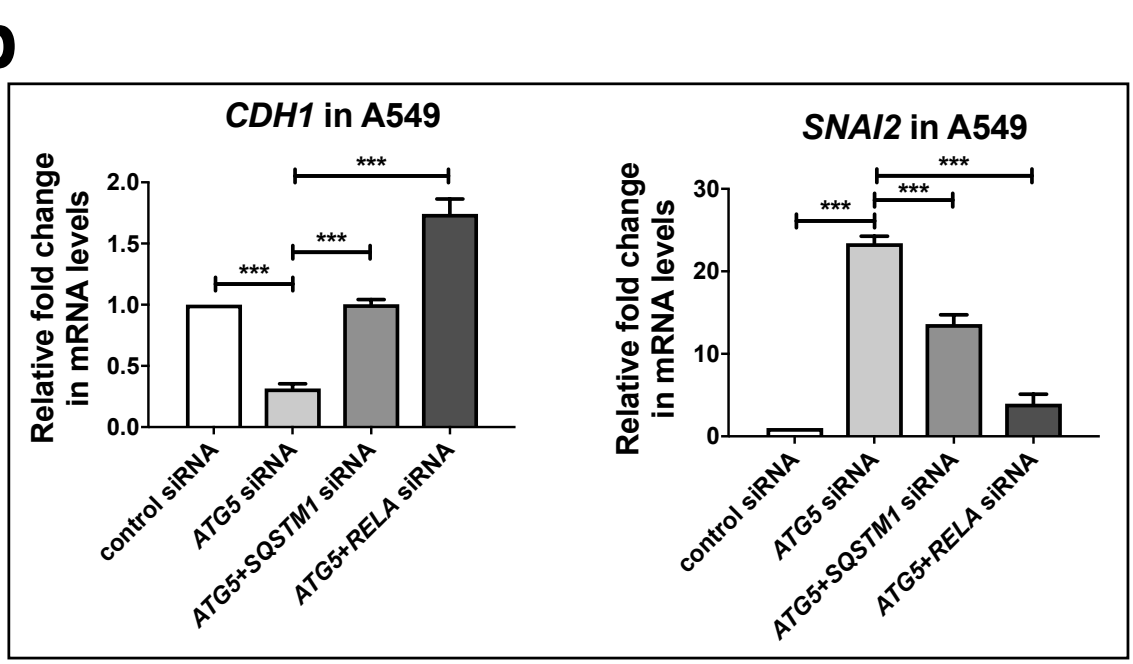

Supplementary Figure 6